The decompression of volatile-poor basaltic magma from a dike into a horizontal subsurface tunnel

A.-M. Lejeune [1], A.W. Woods [2], R.S.J. Sparks [1], B.E. Hill [3], and C.B. Connor [3]

1. Centre for Environmental and Geophysical Flows, University of Bristol, Bristol BS8 1RJ,UK
2. BP Institute for Multiphase Flow, University of Cambridge, Cambridge CB3 OEZ, UK
3. Center for Nuclear Waste Regulatory Analyses, Southwest Research Institute, San Antonio, Texas 78238-5166, USA

ABSTRACT

We examine the flow conditions that likely result if basaltic magma ascending a vertical dike intersects a horizontal subsurface tunnel such as found in an underground radioactive waste repository. Our approach combines theoretical calculations with a series of analog laboratory experiments using viscous syrup. The syrup initially is stored in a vertical Hele-Shaw cell and connected to a high-pressure reservoir, then flows into a low-pressure horizontal tube when a gate connecting the tube to the cell is opened. Although the syrup rapidly advances into the tube, the leading edge of the flow may include a substantial gravity slump zone. The geometry of this slump zone is controlled by the speed of the flow, the size of the tunnel, and the viscosity of the fluid. A quantitative model is developed and tested successfully with the experimental observations. The model is used to calculate the flow conditions that might occur if a volatile-poor magma intersects a tunnel with dimensions comparable to those proposed for the Yucca Mountain, Nevada, repository. During typical flow conditions, with pressures of 5–10 MPa driving the flow, the model indicates that magma would advance along the tunnel at speeds on order of 10 m/s, with the leading 30–60 m of the flow only partially filling the tunnel and propagating as a gravity slump into the tunnel.

1 INTRODUCTION

Humans continue to place communities and critical facilities in potentially hazardous volcanic areas. Increasingly, scientists are being asked to determine the likelihood of a future volcanic event and the resulting public health and safety hazards from a range of potential events. These hazard analyses often need to consider a variety of complex interactions between engineered systems and igneous processes. Igneous events create physical conditions that are often beyond the design basis of most engineered systems, with little data available for direct analysis. In addition, interactions with engineered systems can change the character of an igneous event in ways that never occur in nature. These potential changes in process may directly affect the impact of the resulting hazard. In this study, we will examine the potential changes in magma-flow processes that might occur when rising magma intersects open, subsurface structures such as tunnels or drifts. Results of this investigation will help determine the extent and duration of decompression-induced subsurface flow for low volatile content magmas, and the resulting subsurface hazard.

The United States has generated approximately 40,000 metric tons of high-level radioactive waste from commercial and defense reactors. The current proposal is to dispose this waste in 300-m-deep tunnels beneath Yucca Mountain, Nevada, USA. The regulatory framework in the United States establishes limits on potential doses to the public for a period of 10,000 years (NRC, 2001). This proposed site, however, is located in a geologically active basaltic volcanic field, where the probability of a new volcano forming at the proposed repository site is calculated at 10^{-4} to 10^{-3} during the next 10,000 years (e.g., Connor et al., 2000; U.S. Department of Energy, 2001). Federal regulations require a detailed hazard analysis for all natural events with a greater than 10^{-4} in 10,000 year likelihood of occurrence (U.S. Environmental Protection Agency, 2001). An important component of this hazard analysis is how flow processes may be affected if ascending magma intersects 5-m-diameter tunnels containing

radioactive waste. The actual dike-tunnel interaction mechanism will depend on regional and local stress relationships between the tunnels and surrounding rock. A future dike rising beneath the proposed repository, however, would likely intersect multiple tunnels located 20–80 m apart, as the tunnels are oriented roughly orthogonal to the direction of maximum horizontal compressive stress and thus orthogonal to the direction of dike propagation (e.g., Delaney et al., 1986; Morris et al., 1996). Clearly, confined basaltic magma intersecting a tunnel at essentially atmospheric pressure would decompress and flow into that tunnel. The potential for release of radioactive waste into the accessible environment, however, will be controlled by the conditions of initial and sustained magma flow on waste containment systems. The purpose of this study is to improve understanding of the flow conditions that may occur during rapid decompression of a volatile-poor basaltic magma.

This study is also relevant to other countries where geological disposal of radioactive waste is being considered in volcanically active areas. In addition to radioactive waste repositories, igneous disruption of other subsurface facilities can present credible hazards. For volcanically active areas such as Auckland, New Zealand (Johnston et al., 1997), rising basaltic magma may intersect subsurface structures including utility, sewage, and communications lines. Decompression flow into these structures may be more extensive than modeled with a simple dike geometry, thereby increasing the amount and duration that essential services are disrupted. Although such disruptions have a low probability of occurrence, the resulting hazard may be relatively high if hazardous materials are released or critical infrastructure is damaged.

To examine the flow regimes ensuing from a potential disruption of the repository by high-pressure basaltic magma ascending along a dike, we have developed a simple theoretical model of the time-dependent viscous flow based on a rather simplified geometry of the dike-tunnel system and dimensional scalings of the different forces involved in the subsurface environment. We then designed an analog

experimental model for this system, which is described in section 3. In section 4, we present some of the results of our experiments, examining how the flow rate depends on the pressure drop into the tunnel and describing the morphology of the flow front. We also compare these results with the theoretical model. Finally, in section 5, we return to the scale of the subsurface repository and examine the implications of the model in the context of the proposed Yucca Mountain development. We also comment on the philosophical difficulties of forecasting processes that involve interaction between geological phenomena and manmade structures.

2 BACKGROUND AND CONCEPTUAL MODEL

We have developed a hierarchical program of numerical and experimental investigations to evaluate decompression-induced flow phenomena in the interaction of basaltic magma with a geological repository of radioactive waste with the expected design attributes of Yucca Mountain. Models and experiments in this paper examine flow conditions appropriate for a volatile-poor basaltic magma. Although we recognize that many basalts contain appreciable quantities of magmatic volatiles, we will first establish the underlying principles that control decompression-induced flow without the complications of volatile exsolution and rapid fragmentation phenomena.

Pliocene-Quaternary age basalts in the Yucca Mountain region are mildly alkaline and contain phenocrysts of predominantly olivine and augite, with variable amounts of plagioclase and occasionally titanian pargasitic amphibole (Vaniman et al., 1982; Hill et al., 1995). By comparison with hydrous crystallization experiments on mildly alkaline basalt (e.g., Knutson and Green, 1975), the presence of amphibole phenocrysts indicates initial magmatic water contents of at least 2 weight percent. Such water contents are expected to produce a high-velocity fragmented flow following the rapid decompression at a depth of 300 m (e.g., Bokhove and Woods, 2002). Degassing at the dike front as it ascends toward the

repository, however, could result in a volatile-poor region just behind the tip of the ascending dike. These situations will lead to the flow processes investigated herein. For example, basaltic volcanic eruptions such as occurred in 1975 at Tolbachik Volcano, Russia (Doubik and Hill, 1999) or in 1973 at Heimaey, Iceland (Thorarinsson et al., 1973) started with initial fire-fountaining activity but evolved to more energetic eruptions within 24 hours. This evolution may be related to degassing effects during initial ascent of the magma, suggesting that initial hazards from subsurface flow may be represented by decompression of a volatile-poor rather than volatile-rich magma. In addition, during the course of a basaltic eruption, degassed basaltic magma may intersect tunnels in association with syneruptive dike propagation. Another rationale for investigating the case of volatile-poor magma is that this simpler case would allow us to develop an understanding of flow processes within a hierarchy of models of increasing complexity.

Rising basaltic dikes typically have a fluid pressure on the order of 1–10 MPa in excess of local lithostatic pressure, which allows the magma to ascend from depth, fracture the surrounding rock, and dilate fractures to a 1-m-aperture (Pollard, 1973; Lister, 1991; Lister and Kerr, 1991). At a 300-m-depth beneath Yucca Mountain, the tuff bedrock has a hydrofracture stress of 5.1–5.5 MPa (Stock et al., 1985). In contrast, the proposed repository tunnels would have atmospheric pressure (Rosseau et al., 1999), and thereby provide the path of least resistance for the ascending magma. We therefore anticipate that on intersection of the dike with the tunnel, the magma flow will be diverted into the tunnel.

The design for the proposed high-level radioactive waste repository at Yucca Mountain, Nevada, is currently under development and may change significantly from conditions outlined in this paper. Current plans are to locate approximately 50 horizontal tunnels at depths of 200–300 m below the surface of Yucca Mountain. The east northeast-trending tunnels are approximately 5 m in diameter, 1 km long, and spaced 80 m apart. This tunnel orientation is approximately parallel to the direction of minimum

horizontal *in situ* stress (e.g., Morris et al., 1996). The tunnel system has a footprint of 1 x 5 km, and both ends of each tunnel are connected to the surface by two access tunnels with a diameter of 7–10 m. Radioactive waste will be stored in Cr-Ni alloy canisters up to 2 m in diameter and up to 5 m in length, which will be covered by a Ti-alloy drip shield. Current plans are to seal tunnel ends after waste emplacement and to not emplace backfill around the drip shields. The tunnels will be at one atmosphere pressure and can effectively be considered as empty cavities, as the waste canisters occupy approximately 20 percent of the volume of the tunnel.

For typical magma ascent rates of 1 m/s, flow from each 80-m-long by 1-m-wide dike segment thus can be captured by a 20 m^2 tunnel if the flow accelerates to a speed of 4 m/s as it propagates into the tunnel. An understanding of the resulting hazard potential depends on the actual rate of flow, the effects of flow acceleration on magma supply in the feeder dike, and on the time needed to fill an intersected tunnel and re-establish magmatic pressures.

We now build a simplified model of this process and explore the flow regimes that may develop. We then describe an analog laboratory experiment that has been designed to simulate the flow, and test the model quantitatively. First, it is useful to examine the dimensionless parameters that describe the ratio of forces in the problem and to use these parameters to examine typical flow regimes in operation.

As the flow moves into the tunnel, it experiences a sudden decompression, ΔP, and an associated acceleration. We simplify our model by assuming that in this shallow part of the crust, the crust is sufficiently strong to withstand the decrease in pressure. We therefore assume the flow geometry to be fixed. This assumption simplifies the model, in that following breakthrough, the rapid decompression of the magma may lead to partial closing of the dike and also some failure of the dike walls.

The typical flow speeds in the basaltic dikes prior to breakthrough is on the order of u = 1 m/s, based on both observation and theory (Wilson and Head, 1981; Lister, 1991). For a dike width of w = 1 m, magma of viscosity μ = 30 Pa·s and magma of density ρ = 2,500 kg/m^3, the typical Reynolds number of the flow, $\rho uw/\mu$, is approximately 80. For such a flow, the turbulent drag exerted by the walls of the dike has a magnitude of $2fu^2\rho/w$, where f is the turbulent friction factor, on the order of 0.01. The turbulent drag has a value of approximately 50, whereas the viscous drag acting from the conduit walls has a value of 12 $\mu u/w^2$, which has magnitude of approximately 360. Thus, for the typical flow regime in a dike, the flow is dominated by viscous drag, but the turbulent friction does contribute to the pressure losses experienced by the flow (cf. Wilson and Head, 1981). A rapid decompression of the flowing gas-magma mixture by approximately 1–10 MPa as it breaks into a tunnel will lead to an acceleration of the flow. However, for an incompressible (i.e., volatile-free) magma, the ensuing magnitude of the flow is expected to be similar to the original value. This is because a decrease in pressure on the order of 1–10 MPa at the flow front, as the flow breaks through into the tunnel, increases the effective overpressure by an amount comparable to the original overpressure driving magma flow in the system.

A second important parameter concerns the hydrostatic pressure gradient in the nose of the flow as it spreads down a tunnel. In this nose region, of length L, the hydrostatic pressure gradient is represented as $g\rho r / L = 10^5 / L$, where r is the radius of the tunnel. The free surface in the nose region can be maintained only if the hydrostatic pressure gradient is greater or equal to the driving pressure gradient, which is balanced by viscous resistance and turbulent drag. For a flow speed u along the tunnel on the order of 10 m/s, the viscous resistance, which is represented as $8\mu u / r^2$, is on the order of 400 kg/m^{2}s. In contrast, the turbulent drag is represented as $2\rho fu^2$ / r, which has a value on the order of 2,000 kg/m^{2}s. The hydrostatic pressure gradient is therefore comparable to the net frictional resistance if the nose of the flow extends a distance on the order *of* L = 50–100 m. Behind this advancing gravity intrusion, the tunnel will be completely filled with magma.

These relationships establish the balance of forces and the leading order structure of the flow that may arise following breakthrough of degassed magma into a tunnel. We now use these results to develop the analog experimental study of the morphology of this advancing front. We compare the scaling for the extent of the nose of the flow with our experimental data, and we develop and test a model for the continuing flow behind the nose.

3 THE ANALOG EXPERIMENTAL SYSTEM

We developed an analog experimental apparatus to model the flow of magma up a dike and into a horizontal tunnel, with a fixed geometry along the flow path. This apparatus (Figure 1) consists of a vertical Hele-Shaw cell consisting of two parallel aluminum and glass plates that are 200 mm wide and 500 mm high. The 10-mm gap between these plates represents a fixed-geometry dike. The base of the cell is connected to a large cylindrical reservoir that contains pressurized liquid. This reservoir represents a deep magma source that drives magma ascent in the dike. The reservoir has an internal diameter of 153 mm and a height of 485 mm. Near the top of the Hele-Shaw cell there is a hydraulically operated gate. This gate, which opens in a fraction of a second, connects the cell to a horizontal glass tube of 40 mm radius and 450 mm length. The axis of the horizontal tube is normal to the plates of the cell. The whole system is sealed from the air, and the initial pressures at (i) the top of the reservoir above the layer of liquid, (ii) the top of the Hele-Shaw cell, and (iii) the end of the horizontal tube are controlled independently by three vacuum regulators (SMC handle-operated vacuum regulators series T203) connected to a diaphragm vacuum pump (KNF Neuberger model N180.3 FT.18). This configuration enables us to control the pressure difference between the reservoir and the top of the cell and also between the top of the cell and the horizontal tube. Pressures are measured with BOC Edwards active strain gauges (ASG NW16–1000 mbar). These gauges have been calibrated in the Calibration Laboratory

of the Southwest Research Institute and have an accuracy better than ± 1 mbar. A series of miniature pressure sensors (113A21 sensors from PCB Piezotronics) were embedded at equal distances along the bottom of the horizontal tube, to record the changes of dynamic pressure during the flow propagation.

3.1 Experimental Materials

We used three working fluids as analogs to volatile-poor basaltic magma. The primary fluid was pure Golden Syrup, a partially inverted refiners syrup manufactured by Tate & Lyle Company. The syrup contains 31–38 weight percent sucrose, 42–50 weight percent invert sugar, and the remainder is dominantly water. This syrup has a Newtonian rheology with a strongly temperature-dependent viscosity (e.g., White, 1988; Davaille and Jaupart, 1993). To cover a wider range of Reynolds numbers, we also used less viscous liquids: Golden Syrup diluted with 5 and 15 weight percent deionized water, called DGS5 and DGS15, respectively. Viscosities of the samples used in our experiments were measured over a range of shear rates and temperatures between 0 and 40 °C with a Haake RV20 Rotovisco rotating cylinder viscometer, using the sensor systems M5/MVI and M5/SVII. During these measurements, temperatures were set and controlled by a temperature vessel connected to a thermal liquid circulator. Variations in syrup viscosity as functions of water content and temperature are shown in Figure 2. Densities were calculated by weighing different known volumes of each fluid at room temperature.

In the experiments, the flow regimes included slow viscous flows of very small Reynolds number, but also flows in which the Reynolds number was as large as 100. These latter experimental flow conditions are comparable to the likely basaltic flow conditions discussed in the previous section, in which Reynolds numbers for the tunnel, $\rho u r / \mu$, have value on the order of 800. In comparison, Reynolds numbers for the potential dike flow are on the order of 100. However, the slow viscous flow experiments are useful as an analog model of the structure of potential flows into a tunnel, in that they illustrate the

balance of applied pressure and dissipation and the slumping of the flow nose, even though the flow resistance in the tunnel is through viscous dissipation rather than turbulent drag.

4 EXPERIMENTAL RESULTS

Two series of experiments were performed with the experimental apparatus. First, a series of calibration experiments were conducted to examine the initial ascent of syrup up the Hele-Shaw cell as a function of the pressure difference between the reservoir and the top of the ascending layer of syrup. This procedure enabled us to test the model of flow resistance in the reservoir-cell part of the system, independently of the horizontal tube. The second series of experiments involved measuring the flow in the glass tube following the opening of the gate between the horizontal tube and the Hele-Shaw cell. In these experiments, the cell was initially filled with syrup while the gate was closed. The pressure in the tube was then lowered to a prescribed value below that in the cell, and the gate was opened. The rate of advance of the syrup was then measured, and the morphology of the flow front in the tube was recorded by high-speed video.

4.1 Initial Calibration Experiments

We performed a systematic series of experiments to examine the ascent of syrup in the Hele-Shaw cell as a function of the overpressure and the syrup viscosity. In Figure 3, we present data that illustrate the variation of the height of the syrup-air interface in the cell as a function of time. The different curves correspond to different pressure contrasts between the top of the reservoir and the top of the Hele-Shaw cell. In each case, the syrup gradually ascends through the cell to a final, static steady-state in which the difference in pressures between the top of the cell and the top of the reservoir is accommodated by the difference in the head between the reservoir and the cell.

We now present a simple quantitative model of this experiment. For reference, the key parameters used in the model are illustrated in the schematic of the experimental apparatus shown in Figure 1. For the pure Golden Syrup experiments, with flow speeds $u = 0.01$ m/s, the Reynolds number $\mathrm{Re} = uw/\nu = \rho uw/\mu$ based on the width of the cell, $w = 0.01$ m, and the dynamic viscosity given in Figure 2 has value in the range of $\mathrm{Re} = 10^{-3}$–10^{-2}. Thus, we expect inertia to be negligible. Therefore, the flow satisfies the approximate equation for the flow, averaged across the width of the cell

$$u = -\left(\frac{w^2}{12\mu}\right)\left(\frac{dp}{dy}+\rho g\right) \tag{4.1}$$

which applies in the limit of low Reynolds number (Batchelor, 1967), p represents the pressure, and the y-axis is the direction of the flow. Equation (4.1) leads to the relation

$$\frac{dh^2}{dt} = \left(\frac{w^2}{6\mu}\right)(\Delta p - \rho g h) \tag{4.2}$$

where $u = \mathrm{d}h / \mathrm{d}t$, $h = h(t)$ is the vertical position of the ascending flow front in the cell and Δp is the total pressure drop from the base of the cell to the top of the layer of syrup. This pressure decrease has a value given by

$$\Delta p = \Delta p_0 - \frac{\rho g A_c h}{A_r} \tag{4.3}$$

because the depth of syrup in the reservoir decreases by an amount $(A_c h) / A_r$, where A_c and A_r are the cross-sectional areas of the cell and the reservoir. Equations (4.2) and (4.3) lead to the relationship between the ascent height h and time t

$$\left(\left(\frac{\Delta p_0}{(\lambda\rho g)^2}\right)\ln\left(\frac{\Delta p_0}{\Delta p_0-\lambda\rho g h}\right)\right)-\frac{h}{\lambda\rho g}=\frac{w^2 t}{12\mu} \tag{4.4}$$

where $\lambda = 1+A_c/A_r$. Figure 3 compares the experimental data with the expected values calculated from Equation (4.4), and we find very good agreement for each experiment. Equation (4.4) also identifies that the early time rate of increase of the depth of the cell is given by

$$h^2 = \frac{\Delta p_0 w^2 t}{12\mu} \tag{4.5}$$

which illustrates how the flow rate initially slows down with time as the head driving the flow decreases.

4.2 Experiments of Flow into a Horizontal Tube

In Figure 4, we present a series of profiles of the flow front as captured from video, which illustrate the propagation of the pure Golden Syrup along the horizontal tube following the opening of the gate. Figure 4a shows a photograph from one representative experiment, with a pressure difference of 20 kPa driving the flow. Figure 4b shows the profiles obtained by tracing the shape of the flow front at successive times during four different experiments ranging from 10–80 kPa pressure difference between the reservoir and the end of the horizontal tube. With larger pressure differences and hence larger flow rates, the leading edge of the flow is nearly vertical. With a smaller pressure difference, the head becomes more inclined as the gravitational force at the nose of the flow becomes comparable to the pressure-driven flow, and the syrup slumps into the tube. In all cases, however, the shape of the leading edge is essentially invariant with time (Figure 5). In Figure 5, data are shown for a series of experiments in which different values of the pressure difference between the reservoir and the top of the cell were used. In each case, the nose and

tail of the flow front move at constant speed, suggesting that a quasi-steady state is established between the background pressure driving the flow and the gravitational pressure head driving the slumping of the nose. This result implies that the walls of the vertical Hele-Shaw cell exert the dominant resistance to flow, and so the flow rate remains constant.

We now model the dynamics of the flow into the horizontal tube, following the opening of the gate, assuming that the vertical cell is filled with syrup. At each height in the cell, the upward flux has value:

$$Q = -\frac{w^2}{12\mu}\int dx\left(\frac{dp}{dy}+\rho g\right) \tag{4.6}$$

Integrating over the depth of the cell leads to the relation

$$Q = \left(\frac{a\beta w^3}{12\mu H}\right)(\Delta p_1 - \rho g h) \tag{4.7}$$

where Δp_1 is the pressure change between the base of the Hele-Shaw cell and the opening into the tube, a is the length of the cell, and β is a dimensionless constant. The constant β accounts for additional resistance that the flow experiences in the Hele-Shaw cell during a transition from a nearly parallel upward flow to a more focused radial flow in the vicinity of the horizontal tube. Detailed calculation of the value of β would require a full three dimensional model of flow in the apparatus, particularly as flow migrates into the horizontal tube. These calculations are beyond the scope of this study. We therefore use equation (4.7) to determine the value of the β for the experiments described below.

Parameter β depends primarily on the width of the cell compared to the width of the tube opening, which determines the degree of flow focusing. Parameter β also depends on the length-to-width ratio of the cell, which determines the fraction of the overall flow path over which the flow is focused. The focusing will

occur over a length scale along the cell comparable to width a. In this region, the resistance to flow will increase as the flow migrates through a progressively smaller area of the cell and hence at a greater speed. Because β may be interpreted as a measure of the reduction in the flow rate associated with this flow focusing, we expect it to have a value somewhat smaller than 1 in the experiments. Scaling the model to a possible dike-repository system, we expect that H is approximately 10–30 km whereas a is approximately 20–80 m. Thus, the effect of this focusing will be negligible, suggesting that $\beta = 1$ would be a good approximation.

Depending on the volume flux and the viscosity of the fluid, flow in the horizontal tube may be dominated by the applied pressure with little gravity slumping at the nose. Conversely, flow may include an extensive gravity driven head that only partially fills the tube. In either case, in the region where the horizontal tube is completely filled with fluid, the pressure gradient is to good approximation related to the flow according to the relation

$$Q = -\left(\frac{\pi r^4}{8\mu}\right)\frac{dp}{dy} \tag{4.8}$$

where r is the tube radius. Integrating along length L of the horizontal tube that is completely filled with fluid, we find the volume flux of fluid into the tube, Q, as a function of Δp_2, the pressure drop along the tube:

$$Q = \frac{\Delta p_2 \pi r^4}{8\mu L} \tag{4.9}$$

In the experiments, the total pressure drop

$$\Delta p = \Delta p_1 + \Delta p_2 \tag{4.10}$$

is controlled because ahead of the point $x = L$ in the horizontal tube the fluid has a free surface on which the pressure equals that in the far-field of the reservoir. Combining equations (4.7) and (4.9), we obtain the governing relation

$$\Delta p = \Delta P_d + \rho g H = Q\mu\left(\frac{8L}{\pi r^4} + \frac{12H}{\beta a w^3}\right) + \rho g H \tag{4.11}$$

where ΔP_d is the overpressure that drives the flow. Here we have used the result that, by mass conservation, the net volume flux in the horizontal tube and in the Hele-Shaw cell is equal. The mean velocity of the fluid front that completely fills the area of the horizontal tube, $u = dL / dt$, is related to the volume flux in the tube according to the relation:

$$\frac{dL}{dt} = \frac{Q}{\pi r^2} \tag{4.12}$$

Also, the over-pressure driving the flow (Equation 4.11) decreases from the initial value ΔP_0 as fluid invades the tube and the level in the main reservoir decreases:

$$\Delta P_d = \Delta P_0 - \frac{\rho g L A_T}{A_R} \tag{4.13}$$

Combining equations (4.11) and (4.13), and integrating, we find that the horizontal extent of the fluid front that completely fills the tube, $L(t)$, is given by the relation:

$$\left(\frac{8\mu A_R}{r^2 \rho g A_T}\right)\left(L + \left[\left(\frac{\Delta P_0 A_R}{\rho g A_T}\right) + \left(\frac{3\pi r^4 H}{2\beta a \omega^3}\right)\right] \ln\left(1 - \frac{L\rho g A_T}{A_R \Delta P_0}\right)\right) = -t \tag{4.14}$$

At early times, when L is small, or in the case that $\Delta P_0 >> L\rho g A_T / A_R$, so that there is very little change in liquid height in the reservoir and hence pressure at the base of the reservoir. As a result of the flow into the horizontal tube, equation (4.14) has the approximate form:

$$L = \frac{\Delta P_0 \beta w^3 at}{12\mu\pi r^2 H} \tag{4.15}$$

This approximation corresponds to the situation in which the main frictional losses controlling the flow into the horizontal tube are dissipated in the Hele-Shaw cell, and hence in which the extent of the liquid-filled zone in the tube increases linearly.

The experimental data (Figure 5) show that to a very good approximation the flow advances along the tunnel with a constant speed. From equation (4.15), we expect the gradient of the lines, L / t, shown on figure 5, to be proportional to the driving overpressure ΔP_0. Figure 6 illustrates the variation of the gradient of those lines, as measured from figure 5, with overpressure ΔP_0. This variation (Figure 6) confirms that dL / dt is indeed proportional to ΔP_0. According to equation (4.15), the constant of proportionality is given by $\beta w^3 a / 12\mu r^2 H$. By measuring this constant of proportionality from figure 6 and combining this with the dimensions of the experimental system, we find that $\beta = 0.95$. In comparison, the expected value for β is 1.0.

Although this model captures the propagation of the fluid-filled front along the horizontal tube, it does not account for the shape or extent of the gravitational slump zone at the nose of the flow. As described in section 2, the extent of this slump zone, D, is determined by a balance between the gravitational pressure gradient, $\rho g r / D$, and the applied pressure gradient, $dp / dz = \Delta p_2 / L$, along the completely fluid-filled part of the horizontal tube. This relationship can be represented as:

$$D \approx \frac{\rho g r}{dp/dz} \tag{4.16}$$

This expression may be re-expressed in terms of the speed of the flow along the tube, u_T, noting that the pressure gradient in the tube is given by $dp/dz = 8\mu u_T / r^2$, leading to the relation:

$$D \approx \frac{\rho g r^3}{8\mu u_T} \tag{4.17}$$

In Figure 7, we compare this expected scaling relationship for the extent of the slumping zone, as given by equation (4.17) and using measurements of the speed of the flow along the horizontal tube, with the laboratory data on the width of the slumping zone. We find reasonable agreement between the expected order of magnitude scaling and the experimental data. Note that the speed u is related to the applied overpressure that drives the flow. In the limit that most of the frictional dissipation occurs in the Hele-Shaw cell rather than the horizontal tube, D can be expressed as:

$$D = \frac{3H\rho g r^5 \pi}{2\beta a w^3 \Delta P_0} \tag{4.18}$$

This expression is equivalent to equation (4.17), because we estimated the value of β using equation (4.15). Equation (4.17) identifies how the length of the gravity intrusion decreases with the overpressure, the width of the cell, and the length of the cell supplying fluid into the horizontal tube. In contrast, the slump zone increases with the radius of the tube and the length of the cell over which the applied overpressure is being dissipated.

4.3 Flows at Higher Reynolds Numbers

The experiments described above refer to low Reynolds number flows in which only the viscous resistance controls the flow dynamics. As discussed in section 2, for a potential repository system, turbulent drag may also be an important process for flows having a higher Reynolds numbers, on the order of 10 to 100. In Figure 8, a series of further experimental results are shown for flows using dilute Golden Syrup of lower viscosity. For these experiments using diluted syrup, Reynolds numbers are on the order of 10 to 100. In comparison, a possible magma flow along a subsurface tunnel will likely have a Reynolds number on the order of 100 to 1,000. In these experiments, an extensive slump zone always develops. The steady slump surface is of comparable length to the horizontal tube. Flow reaches a quasi-steady state only as the fluid reaches the end of the tube. At this stage, fluid is reflected back from the end of the tube and develops a backward-propagating filling front. For higher pressures driving the flow, the front is sharper and more localized as expected, with gravity playing a smaller role in the overall flow.

5 APPLICATION TO POTENTIAL DIKE-REPOSITORY CONDITIONS

We now scale our theoretical model for application to the proposed repository, using representative parameters for magma viscosity and the possible dike-tunnel geometry. In developing the model for application to a geological repository, we draw from section 2 in which we established that the viscous resistance is dominant, but that the turbulent drag, although small, is non-negligible and the Reynolds number of the flow has magnitude in the range of 10–1000. We consider the case of an open tunnel, in which the air has atmospheric pressure ahead of the magma, and a closed tunnel, in which the air gradually becomes compressed as the magma advances and decelerates the flow.

To model this flow regime, we extend the model in section 4 for low Reynolds number flow to include the effects of flow inertia in the model. Flow motion in the dike thus is governed by the equation (cf. Woods et al., 2002):

$$\rho \frac{du}{dt} = -\frac{dp}{dy} - \frac{12\mu u}{w^2} - \frac{c_D \rho u^2}{w} - \rho g \qquad (5.1)$$

Motion in the region of the repository tunnel that is filled with magma is governed by the equation

$$\rho \frac{du_T}{dt} = -\frac{dp}{dz} - \frac{8\mu u_T}{r^2} - \frac{c_D \rho u_T^2}{r} \qquad (5.2)$$

where the speed in the tunnel u_T is related to the speed in the dike according to the relation $u_T = u\,A\,/\,A_T$ where A and A_T are the cross-sectional areas of the dike and tunnel. If the dike extends a vertical distance H, and L is the extent of the tunnel that is fully filled, then equations (5.1) and (5.2) may be integrated and combined to give the relation:

$$\rho \frac{(\lambda L + H) d^2 L}{dt^2} = \Delta p - 4\mu \frac{dL}{dt}\left(\frac{3H}{w^2} + \frac{2\lambda L}{r^2}\right) - c_D \rho \left(\frac{\lambda^2 L}{r^2} + \frac{H}{w^2}\right)\left(\frac{dL}{dt}\right)^2 - \rho g H \qquad (5.3)$$

Here $\Delta p - \rho g H$ is the effective overpressure driving the flow. Equation (5.3) includes both the chamber overpressure and the release of the stress at the level of the repository as the magma flows into the tunnel.

5.1 Open Tunnel Conditions

For potential magma flow into an open tunnel, the pressure ahead of the advancing magma is at atmospheric value. In contrast to the tunnel, the surrounding rock has stress associated with the

overburden of a thickness L_H of rock, although the least principal stress σ_3 may be less than the lithostatic load. However, for simplicity, here we assume the stress is given by the lithostatic head $\rho g L_H$. Because the dike walls and thus the magma in the dike are subjected to this stress, the lithostatic head becomes available to drive the flow into the tunnel. As mentioned in section 2, the model assumes that the walls of the dike are of fixed geometry. Although a fixed geometry is a simplification based on earlier models of conduit flow (Wilson and Head, 1981), it is a reasonable starting point for examining flow into a tunnel following possible intersection by an ascending dike. In practice, the flow may be initially weaker, as the rapid decompression of the magma may lead to temporary closure of the dike walls as a result of elastic strain effects. However, as magma continues to ascend from depth and recompresses the walls of the dike, magma will resume flowing into the tunnel. Our calculations are therefore an upper bound on the flow rates in the system, assuming that the dike wall geometry remains constant during the process.

We solved equation (5.3) numerically based on the assumption of a 5-m-diameter tunnel being fed by a 1-m-wide dike of 80 m lateral extent and supplied from a source reservoir below a brittle-ductile transition zone at approximately 10 km. We assume that at this depth, the ascending magma has an overpressure ΔP, comparable to the strength of the wall-rock, of 5 MPa. We take L_H to have a value of 300 m, and the drag coefficient c_D to have a value of 0.01 (Wilson and Head, 1981). Finally, we take the value 30 Pa·s for the viscosity of the basaltic magma. As in the syrup experiments, the drag in the tunnel is negligible compared to drag in the dike.

Figure 9 shows the steady-state velocity calculated by this model as a function of the overpressure released when the flow invades the tunnel. For the typical range of overpressures, the flow accelerates by a factor of 2–3 compared to the original speed in the dike. Figure 9 also illustrates the length of the gravity slump zone ahead of the steadily advancing magma front as a function of the flow rate in the tunnel. For typical overpressures on the order of 5–10 MPa driving the flow, the gravity slump zone is

30–60 m ahead of the part of the tunnel completely filled with magma. This calculation implies that as the flow develops following breakthrough into the tunnel, magma will spread rapidly along the base of the tunnel over the first few seconds. Subsequently, a nearly steady flow front will become established and advance on the order of 10 m/s down the open-ended tunnel. The shape of this spreading front will be similar to the low-pressure flow regime shown in Figure 4.

5.2 Closed Tunnel Conditions

Tunnels that are proposed to contain high-level radioactive waste may be effectively sealed after waste emplacement. In contrast to an open tunnel, an advancing mass of magma will displace and compress the air between the magma and sealed end of the tunnel. Although rock units in the proposed repository horizons have bulk permeabilities on the order of 10^{-12}–10^{-11} m^2 (Rosseau et al., 1999), these permeabilities are small compared to the 20 m^2 cross-sectional area of the tunnel and thus are neglected in the following discussion. In addition, because the flow speeds are much less than the speed of sound in the air, the air pressure (P_a) essentially will remain spatially uniform. The effective pressure (P_e) will therefore increase inversely with the unfilled volume in the tunnel, according to:

$$P_e = P_a \frac{X}{(X-L)} \tag{5.4}$$

Here X is the length of the tunnel and L is the length of the filled part of the tunnel. The effective pressure driving the flow therefore decreases with time, causing the flow to decelerate. As seen in Figure 10, the effect of the closed tunnel is to cause the simple piston displacement flow to decelerate with time as the air is compressed. While this flow decelerates, the tunnel would continue to fill. However, as the magma slumps along the base of the reservoir, the flow evolves from the simple one-dimensional model presented herein.

6 CONCLUSION AND DISCUSSION

The modeling described in this paper has examined the flow that may develop following breakthrough of a low-viscosity, volatile-poor magma from a dike into a low-pressure subsurface tunnel. We developed both experimental and numerical models of the flow, assuming that the dike-tunnel geometry remains constant. Agreement of the experimental observations with the calculated results of this simplified model suggests that the model captures the first-order behavior of magma flow. A key result from our experimental study is the recognition of a gravitational slumping zone (Figure 4) ahead of the magma front into the tunnel. A simple scaling relationship developed and tested with the laboratory experiments indicates that the length scale of this zone depends on the ratio of the gravitational head across the tunnel compared to the pressure gradient along the tunnel associated with the frictional dissipation of the flow.

We have applied this model to the scale of a proposed radioactive waste repository. For typical overpressures of 5–10 MPa that may be released as the magma flows from a dike into a single tunnel, we calculate a slumping zone develops with a lateral extent on the order of 30–60 m. The speed of the flow along the intersected tunnel is expected to be on the order of 10 m/s.

The model results represent an initial attempt to quantify the processes of magma flow in a tunnel and are based on a number of important simplifications. One key assumption is that the magma does not contain a volatile phase, and therefore the flow is not fragmented. This study thus provides a base case to evaluate the effects of volatiles in other models and experiments. A complementary study described by Woods et al. (2002) explores some of the flow processes that might occur for volatile-rich magma, when a more fragmented, high-velocity flow likely develops on interaction of a dike with a tunnel.

A second key simplification is that the dike-tunnel geometry remains fixed following breakthrough into the tunnel. This simplification is important because as the pressure in the upper part of the dike decreases, the dike may partially close if the magma supply rate cannot match the rate of decompression. However, as magma continues to ascend from depth and the dike-tunnel system is repressurized, the dike would reopen. The present model is therefore likely to represent an upper bound on flow rate into a tunnel for volatile-poor magma.

The creation of anthropogenic hazardous materials such as high-level radioactive waste poses great challenges to societies in trying to evaluate future risks. In the case of a repository for high-level radioactive waste, this evaluation must consider potential hazards that could exist for longer than the span of recorded human history. Thus, scientists are required to assess the interactions of long-term geological processes with engineered systems to help evaluate risks to society for millennia to come. There are geological events of low probability and high hazard, such as large meteor impacts or Volcanic Explosivity Index 8 eruptions, which have never been witnessed but can be clearly deduced from the geological record. This record also provides a basis to assess models that attempt to evaluate physical processes that are not well preserved in the geologic record. In the case of proposed radioactive waste repositories, however, disruption of underground engineered systems by igneous activity has never occurred in the past and geologic analogs are absent. Although the probabilities of igneous disruption are relatively small for the proposed repository site at Yucca Mountain, Nevada, the potential radiological hazard from such disruption appears large relative to other higher probability events and processes (e.g., CRWMS M&O, 2000). Thus, models for this potential disruption must be developed, so that risks can be assessed appropriately. The numerical models developed herein capture the important, first-order processes of flow and are sufficiently general so that they can be tested against observations of natural or experimental flows. Experimental tests support the fundamental results of the numerical models, and provide a basis for use of the models in evaluating long-term risks to public health and safety.

ACKNOWLEDGMENTS

Detailed reviews by Stefan Mayer and Wes Patrick greatly improved the content and readability of this report. The authors thank Mike J. Dury and Fred Wheeler, who helped design and build the experimental apparatus in the workshop of the Earth Sciences Department, University of Bristol, UK. Melissa Hill, Jerry Nixon, and Alan Jenkinson also are thanked for their support and assistance in the laboratory, and we thank Rebecca Emmot for clerical support and Jim Pryor for editorial review. Documentation on the details of the model calculations is available from the authors. R.S.J. Sparks thanks the Natural Environment Research Council (NERC) for a NERC Professorship. This report was prepared to document work performed by the Center for Nuclear Waste Regulatory Analyses (CNWRA) for the U.S. Nuclear Regulatory Commission (NRC) under Contract No. NRC–02–97–009. The activities reported here were performed on behalf of the NRC Office of Nuclear Material Safety and Safeguards, Division of Waste Management. The report is an independent product of the CNWRA and does not necessarily reflect the views or regulatory position of the NRC.

REFERENCES

Batchelor GK, (1967) An introduction to fluid dynamics. Cambridge University Press, Cambridge, pp. 1-615

Bokhove O, Woods AW (2002) The explosive decompression of basaltic magma into a sub-surface repository. Memorandum 1616 of the Mathematical Communications of the Faculty of Mathematical Sciences of the University of Twente, ISSN 0169-2690, pp.1-18

Connor CB, Stamatakos JA, Ferrill DA, Hill BE, Ofoegbu GI, Conway FM, Sagar B, Trapp J (2000) Geologic factors controlling patterns of small-volume basaltic volcanism: Application to a volcanic hazards assessment at Yucca Mountain, Nevada. J Geophys Res 105:417-432

CRWMS M&O (2000) Total System Performance Assessment for the Site Recommendation. TDR–WIS–PA–000001 Rev. 00, ICN 01. DOE Yucca Mountain Site Characterization Office, North Las Vegas, Nevada

Davaille A, Jaupart C (1993) Transient high-Rayleigh-number thermal convection with large viscosity variations. J Fluid Mech 253:141-166

Delaney PT, Pollard DD, Ziony JI, McKee EH (1986) Field relations between dikes and joints: Emplacement processes and paleostress analysis. J Geophys Res 91(B5):4920-4938

Doubik P, Hill BE (1999) Magmatic and hydromagmatic conduit development during the 1975 Tolbachik Eruption, Kamchatka, with implications for hazards assessment at Yucca Mountain, Nevada. J Volcanol Geotherm Res 91:43-64

Hill BE, Lynton SJ, Luhr JF (1995) Amphibole in Quaternary basalts of the Yucca Mountain region: significance to volcanism models. Procedings, Sixth Annual Internationl High-Level Radioactive Waste Management Conference. American Nuclear Society, La Grange Park, IL, pp. 132-134

Johnston DM, Narin IA, Thordarson T, Daly M (1997) Volcanic impact assessment for the Auckland Volcanic Field. Technical Publication Number 79. Auckland Regional Council, Auckland, New Zealand, pp. 1-208

Knutson J, Green TH (1975) Experimental duplication of a high-pressure megacryst/cumulate assemblage in a near-saturated hawaiite. Contrib Mineral Petrol 52:121-132

Lister J (1991) Steady solutions for feeder dikes in a density stratified lithosphere. Earth Planet Sci Lett 107:233-242

Lister JR, Kerr RC (1991) Fluid-mechanical models of crack propagation and their application to magma transport in dykes. J Geophys Res 96(B6):10049-10077

Morris A, Ferrill DA, Henderson DB (1996) Slip-tendency analysis and fault reactivation. Geology 24(3):275-278

Pollard DD (1973) Equations for stress and displacement fields around pressurized elliptical holes in elastic solids. Math Geol 5:11-25

Rosseau JP, Kwicklis EM, Giles DC (1999) Hydrogeology of the Undersaturated Zone, North Ramp Area of the Exploratory Studies Facility, Yucca Mountain, Nevada. Water-Resources Investigations Report 98-4050. U.S. Geological Survey, Denver, CO pp. 1-259

Stock JM, Healy JH, Hickman SH, Zoback MD (1985) Hydraulic fracturing stress measurements at Yucca Mountain, Nevada, and relationship to the regional stress field. J Geophys Res 90(B10):8691-8706

Thorarinsson S, Steinthórsson S, Einarsson Th, Kristmannsdóttir H, Oskarsson N (1973) The eruption on Heimaey, Iceland. Nature 241:372-375

U.S. Department of Energy (2001) Yucca Mountain Science and Engineering Report DOE/RW-0539. U.S. Department of Energy, Office of Civilian Radioactive Waste Management, North Las Vegas, Nevada

U.S. Environmental Protection Agency (2001) Public Health and Environmental Radiation Protection Standards for Yucca Mountain, Nevada. Code of Federal Regulations, Title 40 Chapter 1 Environmental Protection Agency, Part 197. U.S. Environmental Protection Agency, Washington, DC

U.S. Nuclear Regulatory Commission (2001) Disposal of High-Level Radioactive Wastes in a Proposed Geologic Repository at Yucca Mountain, Nevada; Final Rule. Code of Federal Regulations, Title 10 Nuclear Regulatory Commission, Part 63. U.S. Nuclear Regulatory Commission, Washington, DC

Vaniman DT, Crowe BM, Gladney ES (1982) Petrology and geochemistry of hawaiite lavas from Crater Flat, Nevada. Contrib Mineral Petrol 80:341-357

White DB (1988) The planforms and onset of convection with a temperature dependent viscosity fluid. J Fluid Mech 191:247-286

Wilson L, Head JW (1981) Ascent and eruption of basaltic magma on the Earth and Moon. J Geophys Res 86:2971-3001

Woods AW, Sparks RSJ, Bokhove O, Lejeune A-M, Connor CB, Hill BE (2002) Modeling magma-drift interaction at the proposed high-level radioactive waste repository at Yucca Mountain, Nevada, USA. Geophys Res Lett 29(13):1-4

LIST OF PARAMETERS

a	length of cell
w	width of cell
L	length of flow in the filled part of the horizontal tube
r	radius of the horizontal tube
H	vertical extent of flow pathway in cell
h	depth of syrup in cell
h_r	initial depth of syrup in the reservoir
D	extent of the slump zone
A_C	cross-sectional area of the cell
A_R	cross-sectional area of the reservoir
A_T	cross-sectional area of the tube
g	acceleration due to gravity
ΔP_0	initial driving overpressure
ΔP_d	overpressure driving the flow
Δp	total pressure drop from the base of the cell to the top of the fluid layer
Δp_0	initial total pressure drop
Δp_1	pressure change between the base of the cell and the opening into the horizontal tube
Δp_2	pressure drop along the horizontal tube
Q	flow rate
ΔP	pressure difference across flow path, including gravitational head
u	speed in cell
u_T	speed in tube
y	position in the cell, measured upwards
x	position across the cell

z position along the horizontal tube, measured from the cell

β dimensionless scaling factor to account for diversion of flow in cell near horizontal tube

μ viscosity of syrup

ρ density of syrup/magma

Figure captions

Figure 1. Schematic diagram of the analog experimental apparatus, illustrating the key variables.

Figure 2. Viscosity as a function of temperature and water content for pure Golden Syrup (PGS) and Golden Syrup diluted with 5, 10, and 15 weight percent deionized water (respectively, DGS5, DGS10, and DGS15). Temperatures are measured to within 0.1 °C. Each viscosity value was measured and averaged over a range of shear rates.

Figure 3. Rise height of pure Golden Syrup in the Hele-Shaw cell as a function of time, for a series of different applied pressures ranging from 0.55 to 5.5 kPa.

Figure 4. Profile of the syrup-air interface as it flows down the horizontal tube. (a) Photograph of a typical experiment with a 20-kPa pressure difference driving the flow. (b) Tracings of the shape of the leading edge of the flow taken at a series of times in five experiments, with the pressure difference driving the flow being 10, 20, 30, 50, and 90 kPa. In this figure, Δt is the time elapsed between the two consecutive profiles and t_1 corresponds to the time of the first profile after the opening of the gate. To very good approximation, the shape of the head of the flow remains the same as it moves down the horizontal tube.

Figure 5. Variation of the position of the leading and trailing edges of the nose of the flow as a function of time, for applied pressure differences of 20, 30, 50, and 90 kPa driving the flow into the horizontal tube. The speed of the trailing or top edge of the front is shown in Figure 6.

Figure 6. Variation of the speed of the flow front spreading into the horizontal tube as a function of overpressure driving the flow. The data collapse to a straight line to very good approximation, as anticipated by equation (4.15).

Figure 7. Comparison of the idealized scaling law (solid line) for the length of the gravitationally induced slump with experimental observations (dots). In this figure, the calculated length of the slump is evaluated using the speed of the filling front as it advances along the horizontal tube, and the density contrast between fluid in the tube and air.

Figure 8. Three sequences of photographs from experiments using a water-Golden Syrup mixture, with applied pressures of 20, 50, and 80 kPa. The Reynolds numbers of the flows in these experiments are more analogous to those expected for potential magma-repository interactions. For the higher flow rate, the flow front is somewhat irregular but quite localized. For the slower flow rate, the flow front shows more evidence of a gravitational slump region, as in the viscous syrup experiments (Figure 4a), except that the slump region is somewhat more extensive.

Figure 9. (a) Calculated speed of the flow along a proposed repository tunnel as a function of the overpressure released on breakthrough into the tunnel, calculated using equation (5.3). The hydrofracture stress at 300 m below the surface at Yucca Mountain is about 5 MPa, and the lithostatic load at this depth is about 7 MPa. These calculations ignore the influence of any gravity slump zone at the leading edge of the flow. (b) Scaling for the length of the gravity slump zone ahead of the possible tunnel-filling front of magma. The extent of the slump zone is derived from the laboratory experiments, in which the slump zone was calculated accurately by balancing the drag in the horizontal tube with the hydrostatic pressure on the slump surface. In these calculations, the flow is sufficiently fast in the proposed repository tunnel so that turbulent drag rather than viscous friction is dominant.

Figure 10. Calculation of the rate of advance of a planar filling front into a closed tunnel. As the pressure in the tunnel increases, the flow decelerates and the model ceases to apply since the gravity slumping front will dominate the flow.

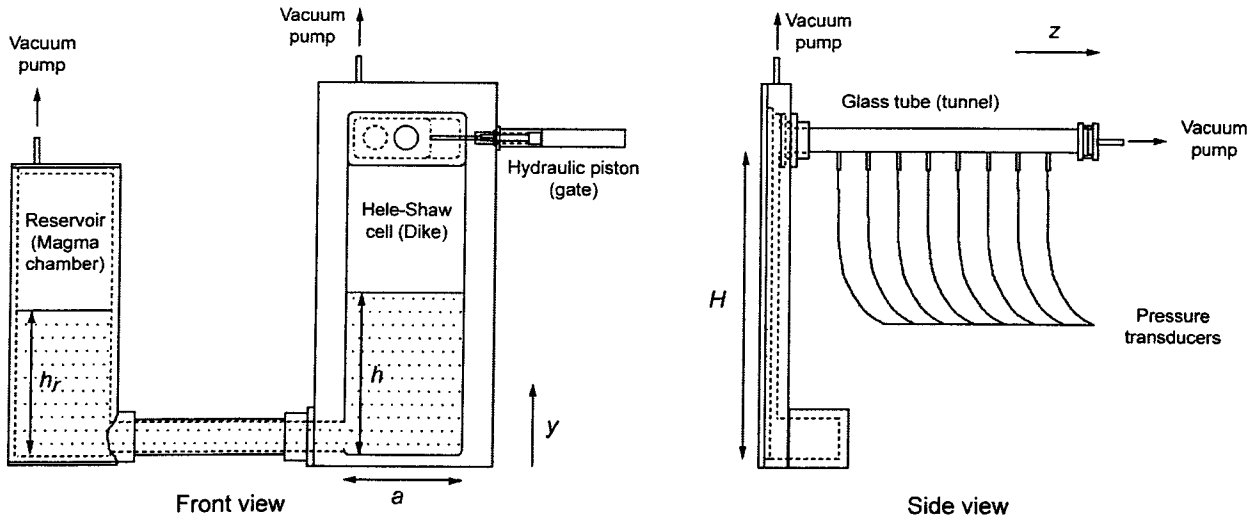
Vacuum pump
Vacuum pump
Reservoir (Magma chamber)
Hele-Shaw cell (Dike)
Hydraulic piston (gate)
h_r
h
y
a
Front view
Vacuum pump
z
Glass tube (tunnel)
Vacuum pump
H
Pressure transducers
Side view

Figure 1

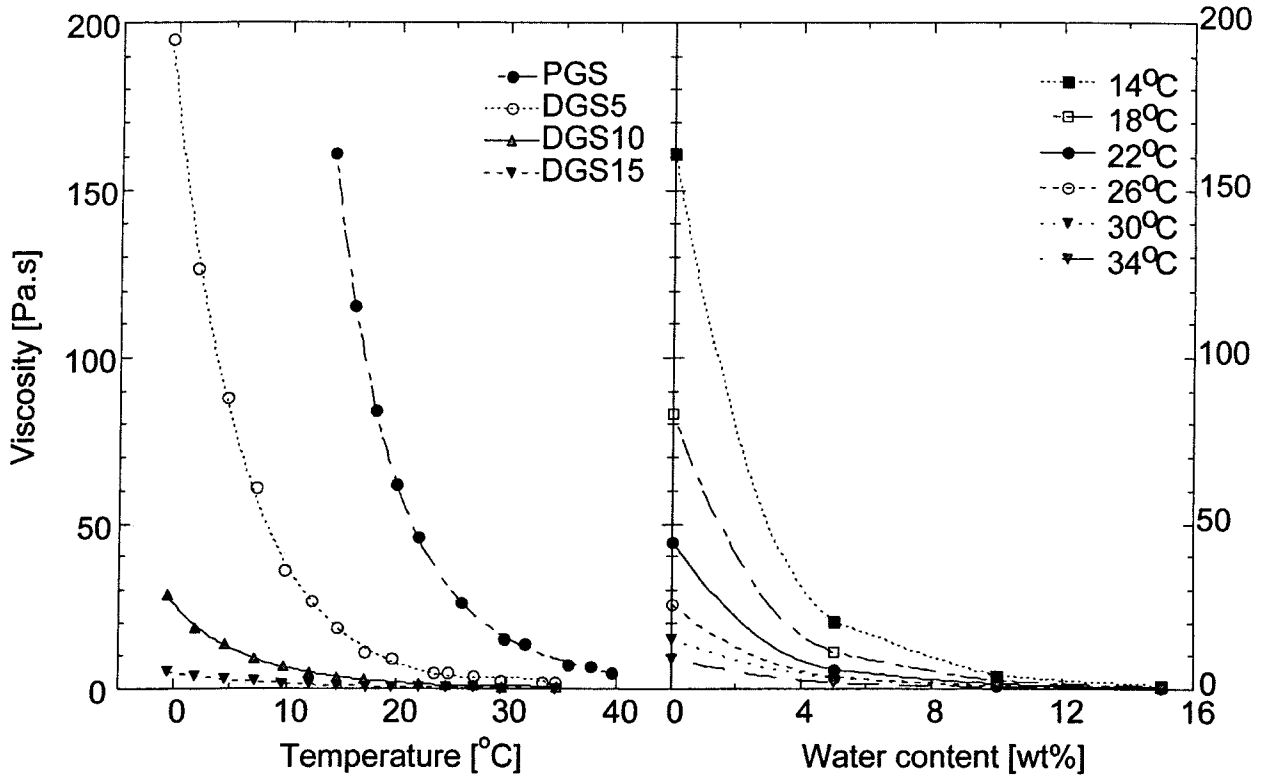
Viscosity [Pa.s]
200
150
100
50
0
0
10
20
30
40
Temperature [°C]
PGS
DGS5
DGS10
DGS15
0
4
8
12
16
Water content [wt%]
14°C
18°C
22°C
26°C
30°C
34°C

Figure 2

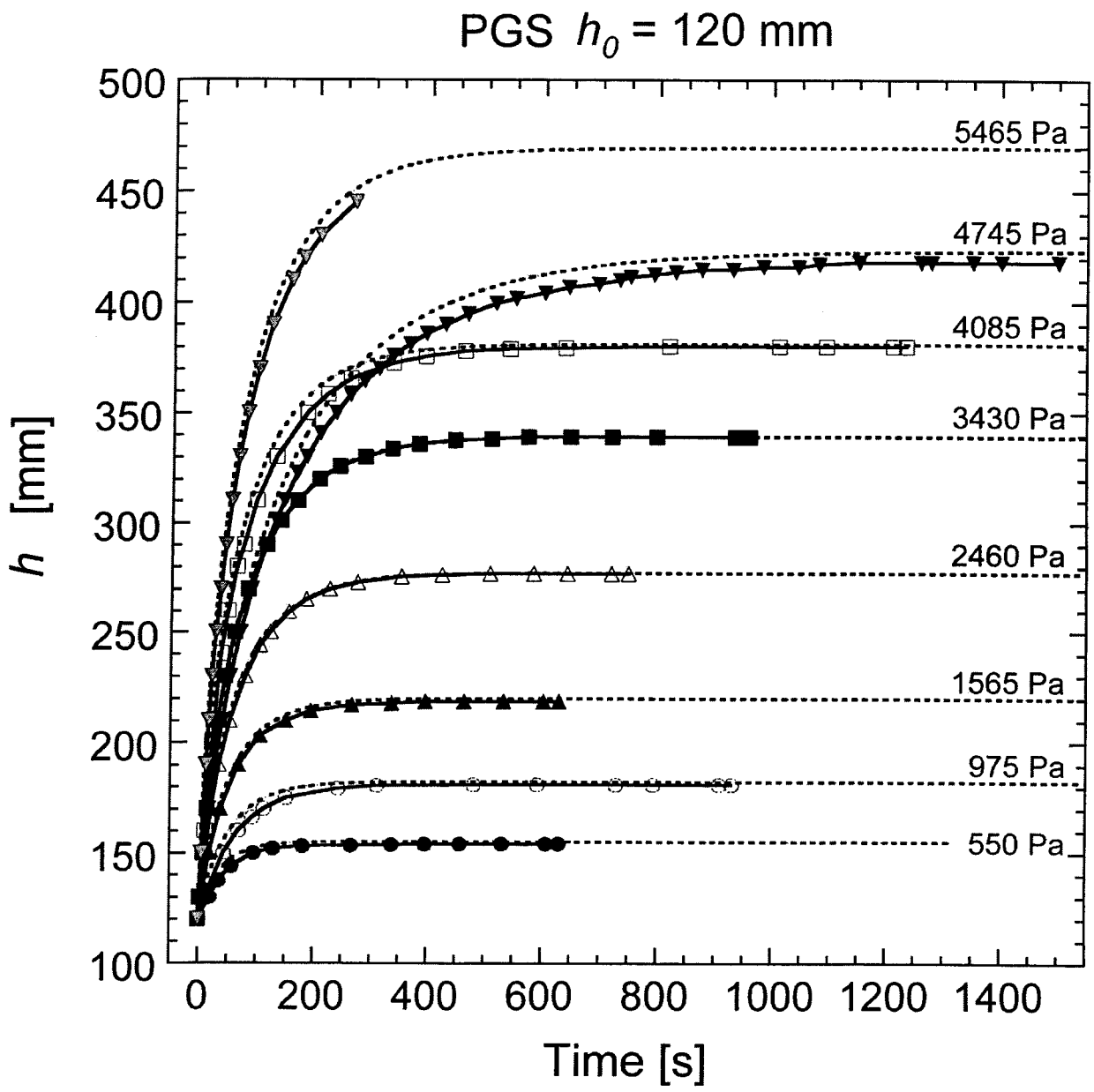
PGS h_0 = 120 mm
500
450
400
350
300
250
200
150
100
h [mm]
0
200
400
600
800
1000
1200
1400
Time [s]
5465 Pa
4745 Pa
4085 Pa
3430 Pa
2460 Pa
1565 Pa
975 Pa
550 Pa

Figure 3

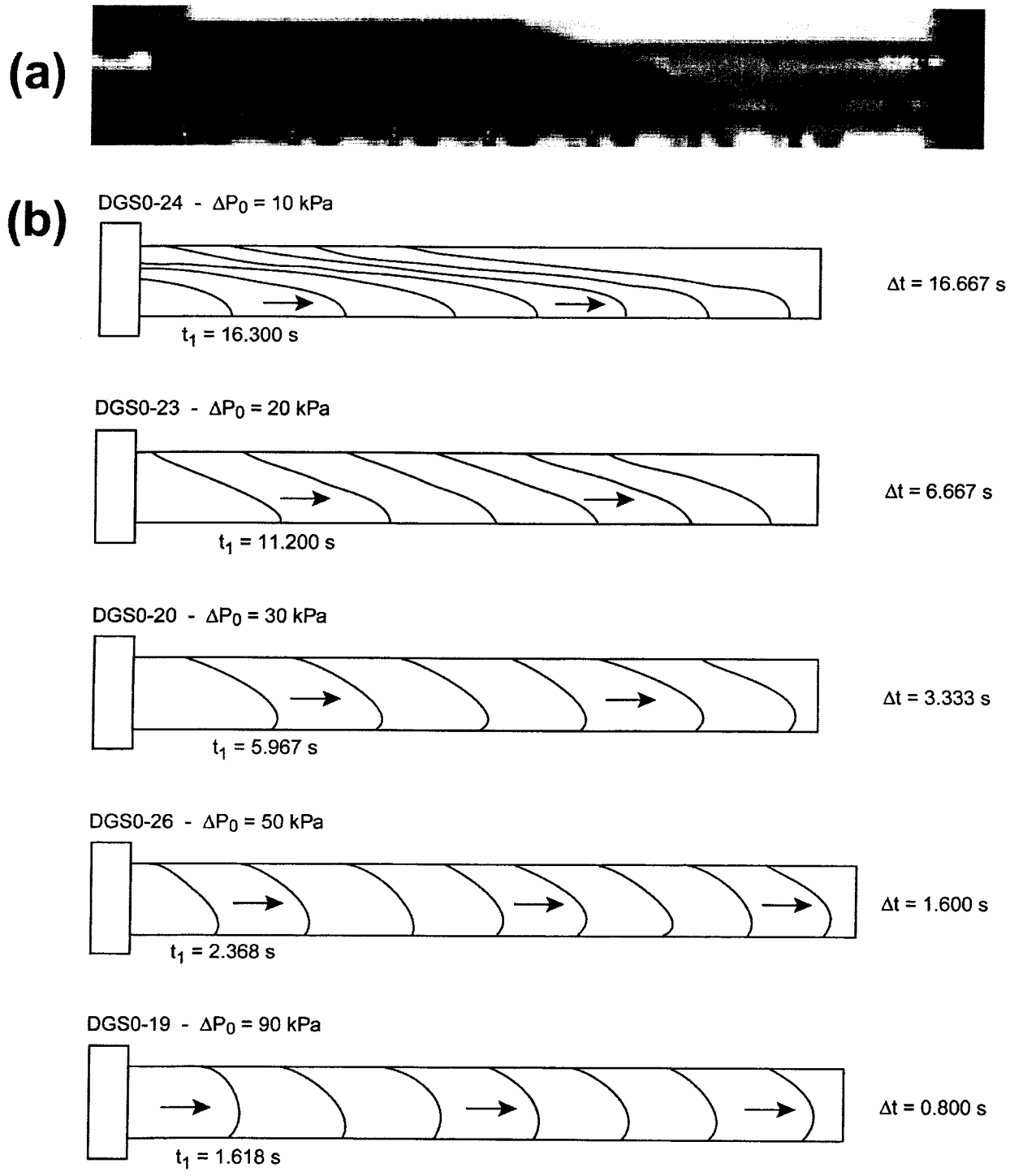
(a)
(b)
DGS0-24 - ΔP0 = 10 kPa
t1 = 16.300 s
Δt = 16.667 s
DGS0-23 - ΔP0 = 20 kPa
t1 = 11.200 s
Δt = 6.667 s
DGS0-20 - ΔP0 = 30 kPa
t1 = 5.967 s
Δt = 3.333 s
DGS0-26 - ΔP0 = 50 kPa
t1 = 2.368 s
Δt = 1.600 s
DGS0-19 - ΔP0 = 90 kPa
t1 = 1.618 s
Δt = 0.800 s

Figure 4

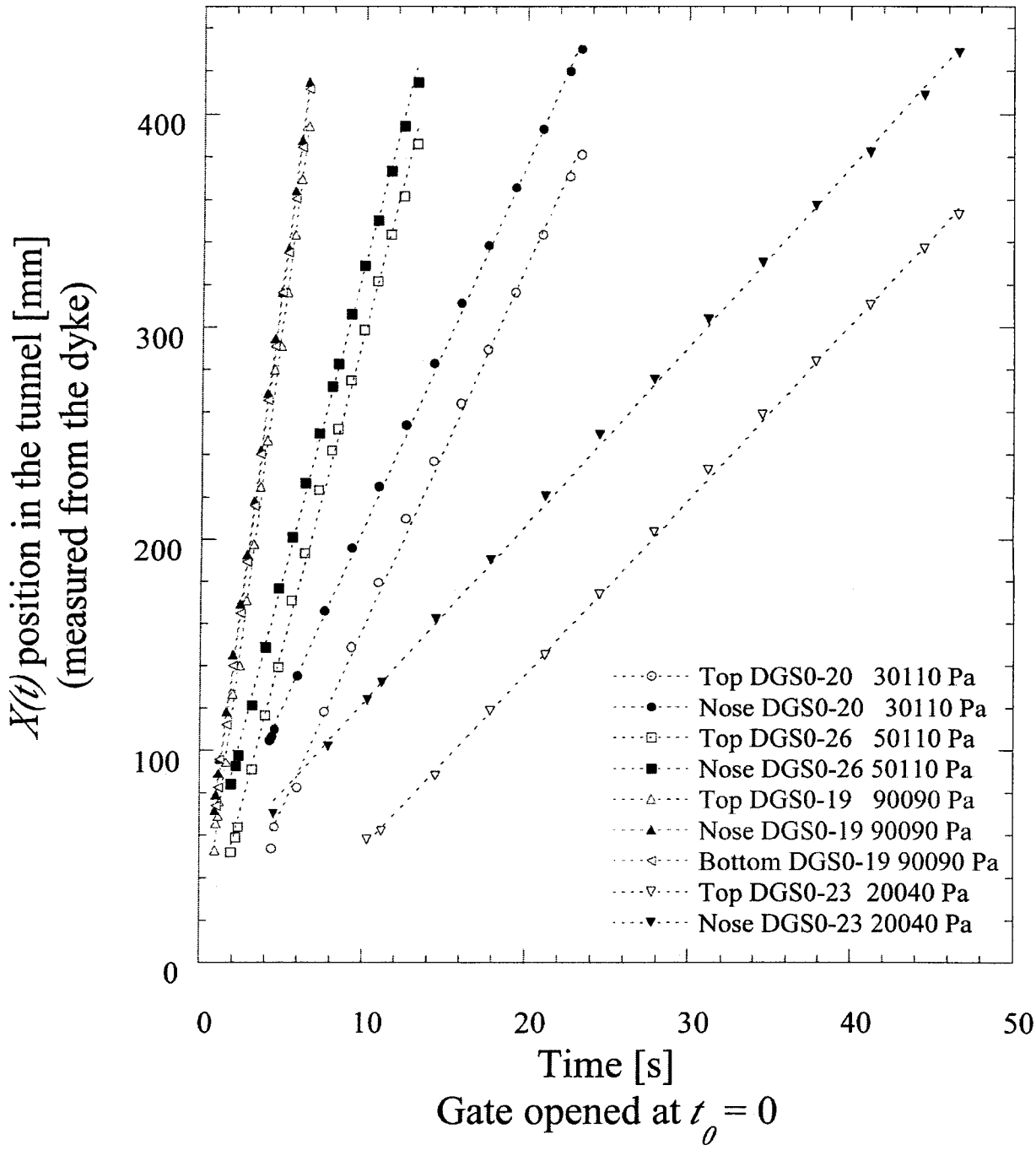
X(t) position in the tunnel [mm]
(measured from the dyke)
0
100
200
300
400
0
10
20
30
40
50
Time [s]
Gate opened at $t_0 = 0$
Top DGS0-20 30110 Pa
Nose DGS0-20 30110 Pa
Top DGS0-26 50110 Pa
Nose DGS0-26 50110 Pa
Top DGS0-19 90090 Pa
Nose DGS0-19 90090 Pa
Bottom DGS0-19 90090 Pa
Top DGS0-23 20040 Pa
Nose DGS0-23 20040 Pa

Figure 5

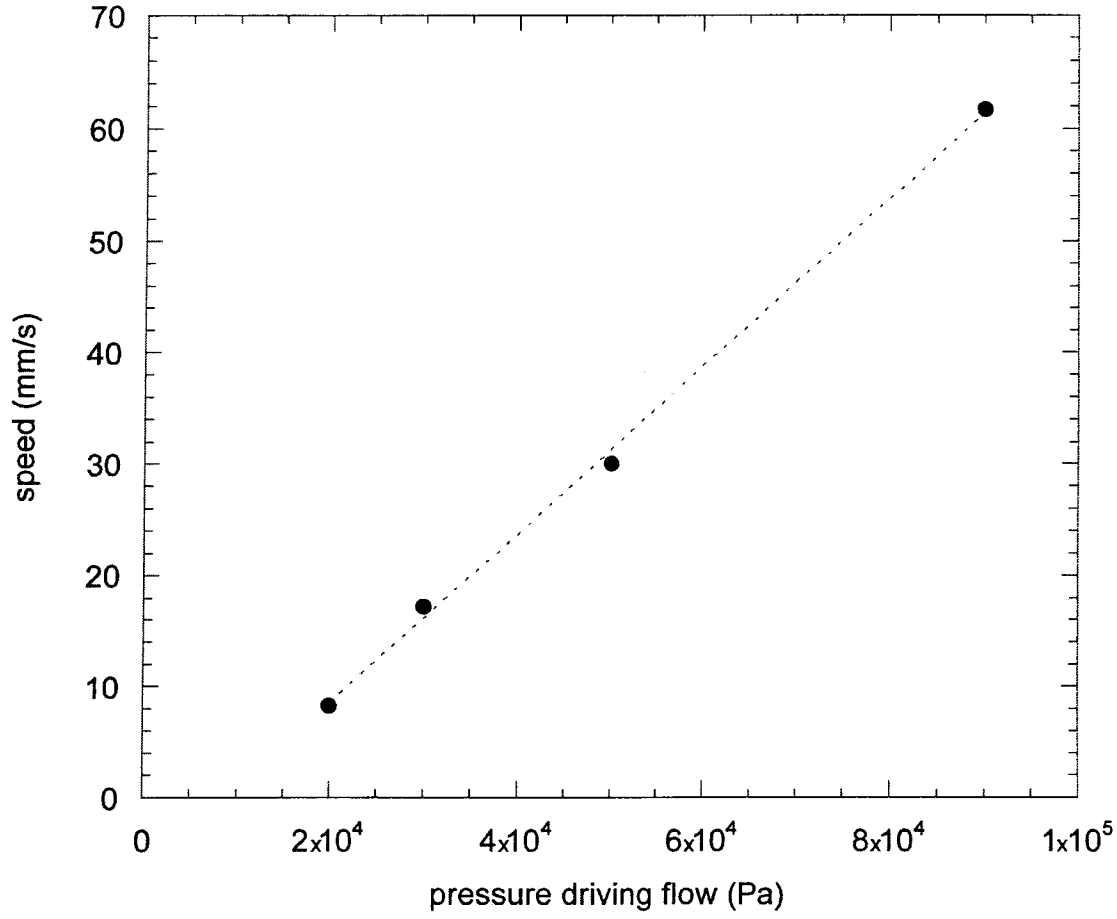
70
60
50
40
30
20
10
0
speed (mm/s)
0
2x10^4
4x10^4
6x10^4
8x10^4
1x10^5
pressure driving flow (Pa)

Figure 6

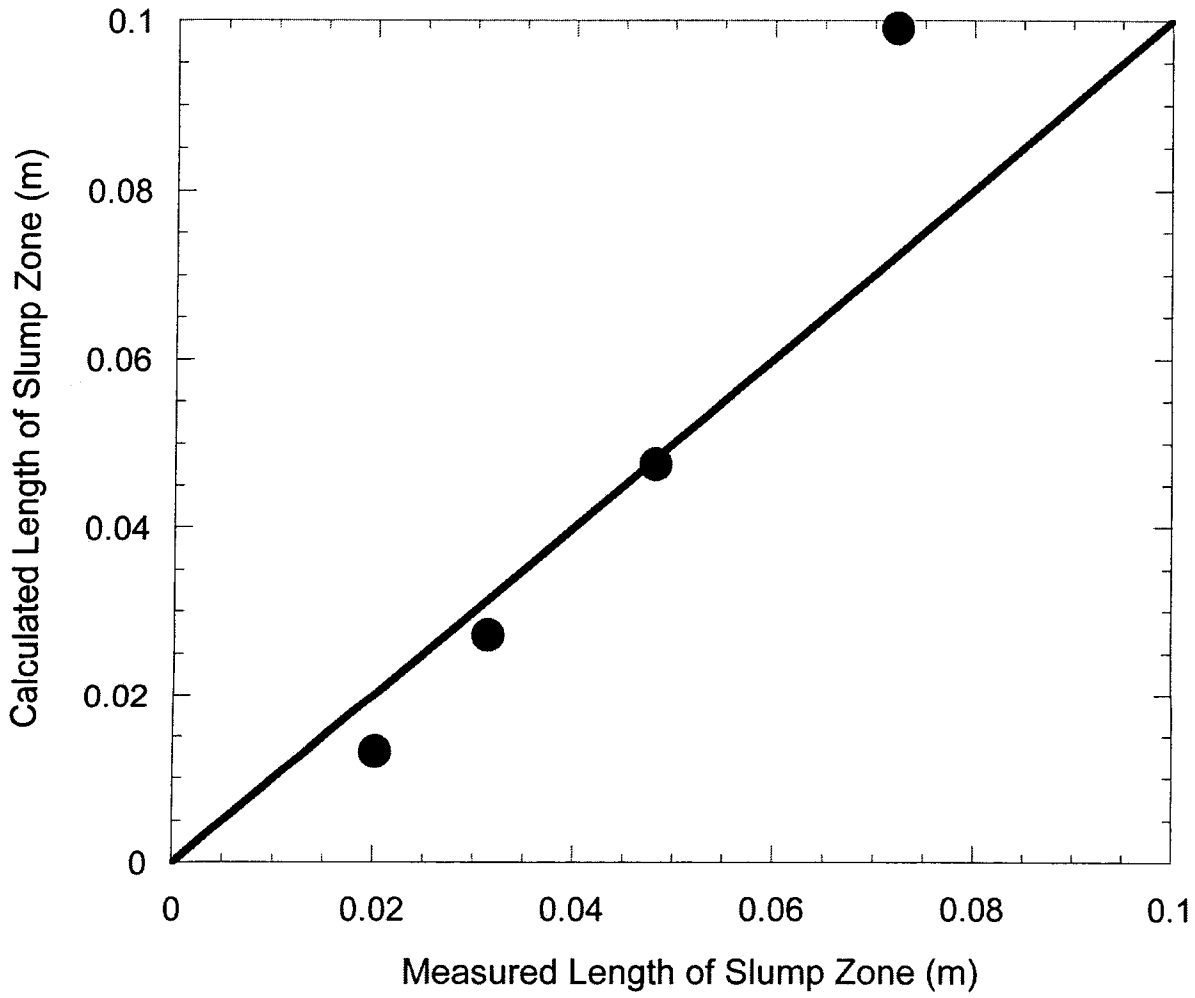
Calculated Length of Slump Zone (m)
0.1
0.08
0.06
0.04
0.02
0
0
0.02
0.04
0.06
0.08
0.1
Measured Length of Slump Zone (m)

Figure 7

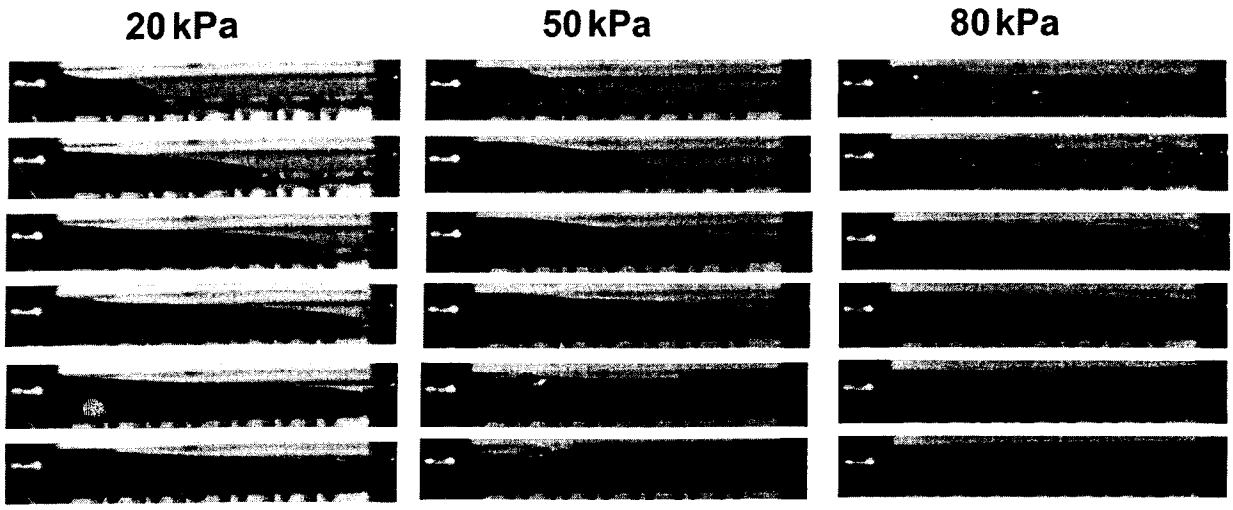

Figure 8

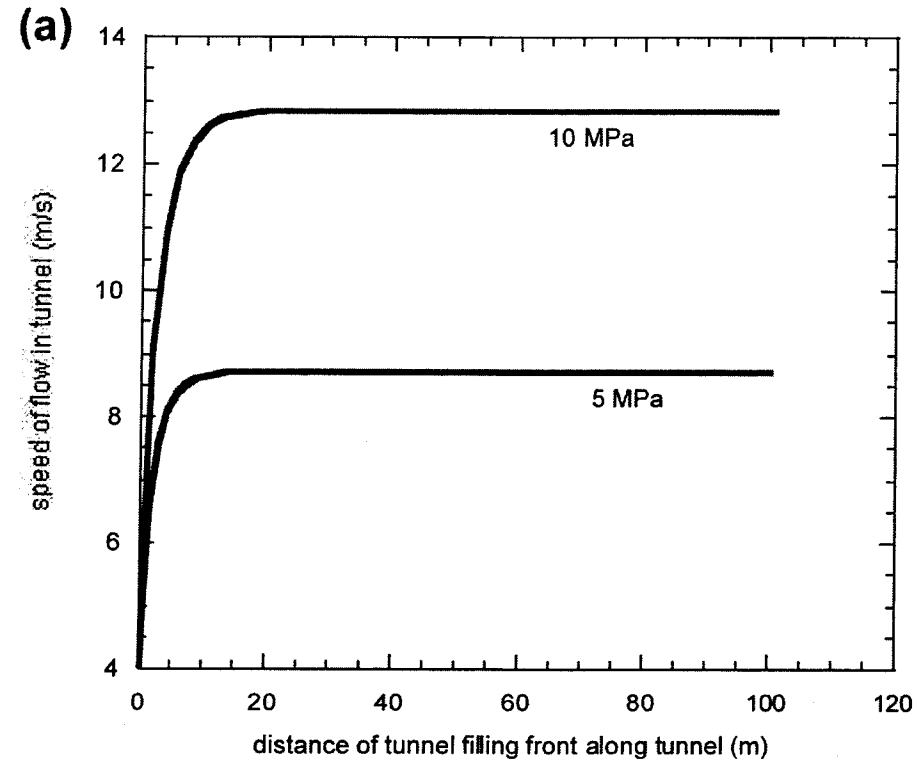
(a)
14
12
10
8
6
4
speed of flow in tunnel (m/s)
10 MPa
5 MPa
0
20
40
60
80
100
120
distance of tunnel filling front along tunnel (m)

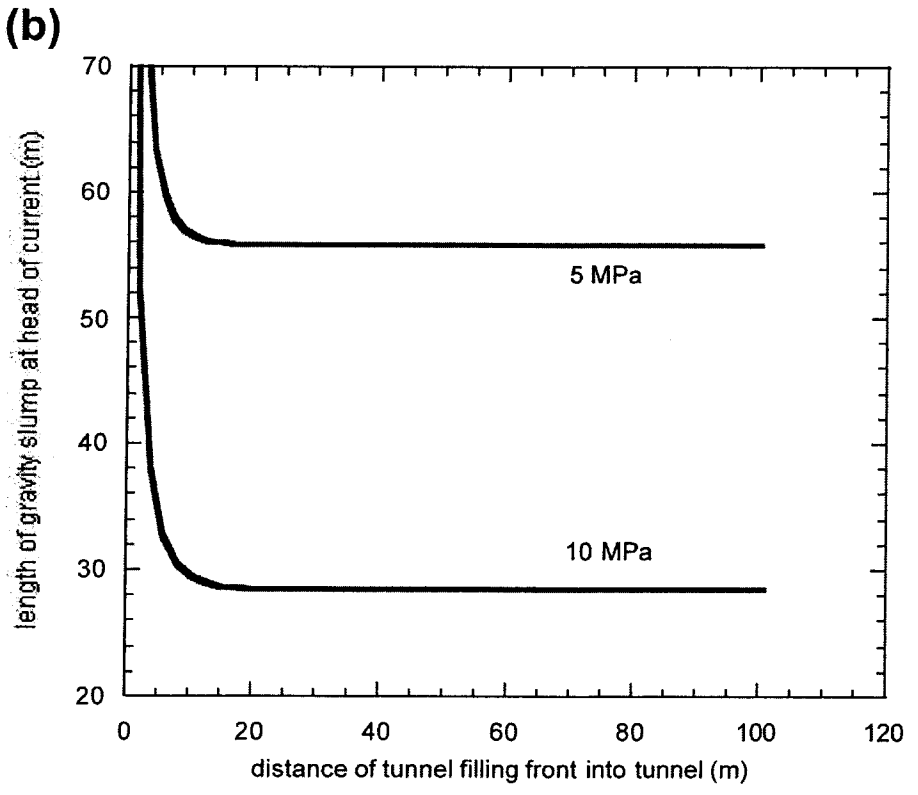
(b)
70
60
50
40
30
20
length of gravity slump at head of current (m)
5 MPa
10 MPa
0
20
40
60
80
100
120
distance of tunnel filling front into tunnel (m)

Figure 9

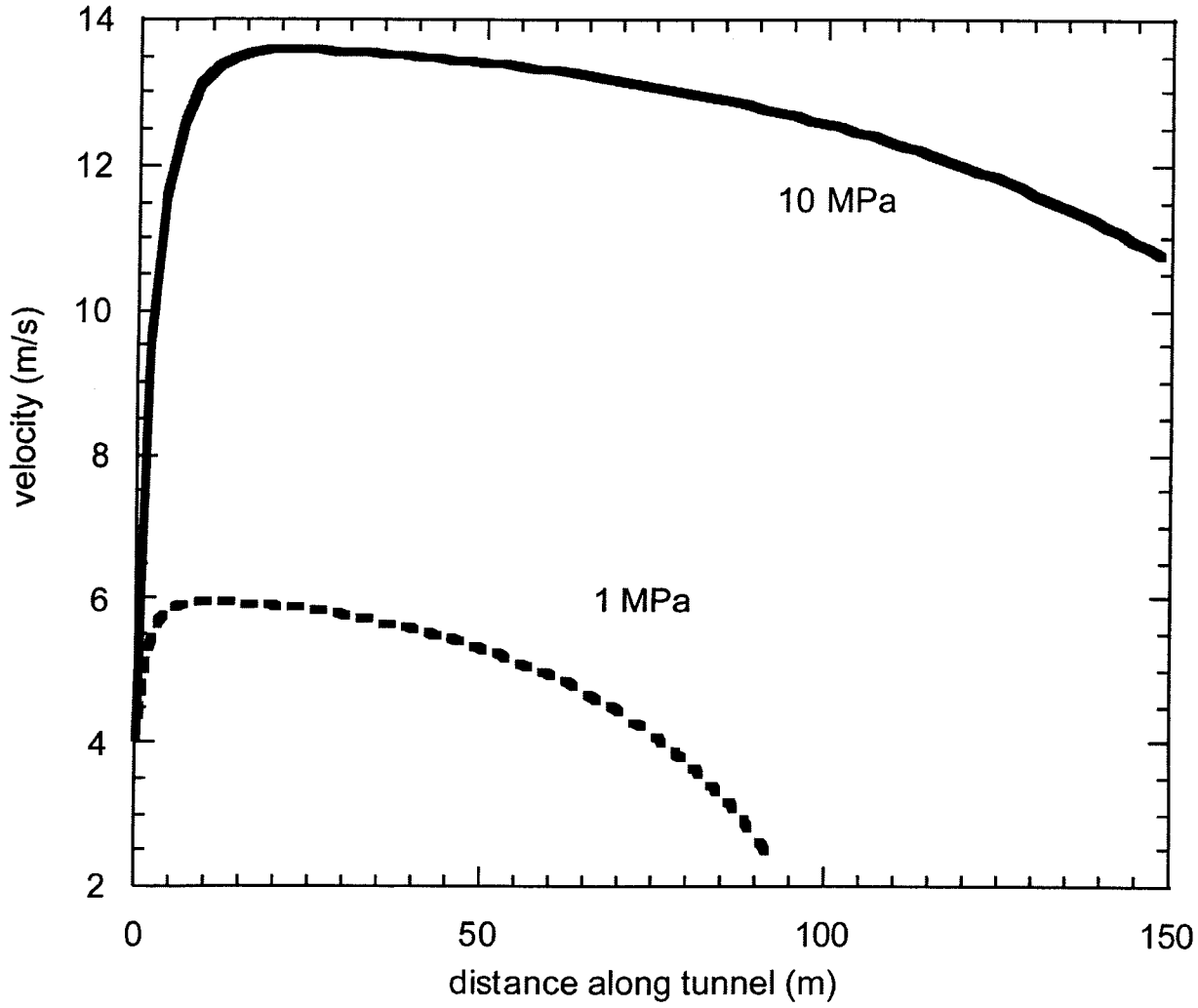
14
12
10
8
6
4
2
velocity (m/s)
10 MPa
1 MPa
0
50
100
150
distance along tunnel (m)

Figure 10